Proceedings of the ASME 2022
Fluids Engineering Division Summer Meeting
FEDSM2022
August 3-5, 2022, Toronto, Ontario, Canada

FEDSM2022-87645

BODY SHAPE EFFECTS ON THE HYDRODYNAMIC PERFORMANCE OF BIO-INSPIRED UNDULATING SWIMMERS

John Kelly
Department of Mechanical and Aerospace Engineering,
University of Virginia
Charlottesville, VA

Yu Pan
Department of Mechanical and Aerospace Engineering,
University of Virginia
Charlottesville, VA

Haibo Dong
Department of Mechanical and Aerospace Engineering,
University of Virginia
Charlottesville, VA

ABSTRACT

In this study, numerical simulations are performed to study the effects of body shape on propulsive performance in a carangiform-like swimming motion. A focus is given to the variation in performance due to changes in the maximum thickness, maximum thickness location, leading-edge radius, and boattail angle of an undulating foil. An immersed boundary method-based incompressible flow solver is implemented to solve for the propulsive performance of two-dimensional undulating foils. The resulting flow simulations yield the thrust, drag, efficiency, and flow for each body shape. From this study, we have found that better propulsive performance comes from a thinner maximum thickness, a maximum thickness location closer to the head of the fish, a narrower boattail angle, and a larger leading-edge radius. Particular care is given to the analysis of the boattail angle, because of the surprising and significant results. In changing only the boattail angle the efficiency is shown to vary by 10.3%. Changes in the leading-edge radius varies the efficiency by 4.4%, the maximum thickness by 4.0%, and the maximum thickness location along the body by 5.0%. The large improvement observed in the thinner boattail angle cases are caused by the increased curvature around the middle of the fish body leading to a high-pressure region at the tail that improves the thrust performance. The results can be used to improve understanding of fish body shapes observed in nature as well as better informing the design of bio-inspired underwater robots.

Keywords: direct numerical simulation, immersed boundary method, bio-inspiration, hydrodynamics

NOMENCLATURE

δ_{max}	maximum thickness
S_{max}	maximum thickness location
α	leading edge radius
β	boattail angle
T	period of motion
λ	wavelength of the motion
Re	Reynolds number
p	hydrodynamic pressure
c	foil chord length
ν	kinematic viscosity
U_∞	freestream velocity
A	tail motion amplitude
f	tail beat frequency
St	Strouhal number
ρ	fluid density
C_T	thrust coefficient
C_P	power coefficient
C_x	x force coefficient
η	Froude efficiency
ω_Z	z – vorticity
C_{pr}	pressure coefficient

1. INTRODUCTION

Recently, scientists have looked to the highly evolved examples given in biology to improve the engineering design of underwater vehicles [1]. By studying the fluid mechanics of fish swimming, the mechanisms that allow them to swim quickly and efficiently can be determined and copied in engineering design. Previous studies have focused on the hydrodynamics of fish as they are seen in nature, investigating a variety of swimming types, geometric features, fin interactions, and other effects on the propulsive performance and wake structures generated by fish swimming [2-4]. Additional studies have been completed utilizing geometric simplifications of fish bodies into two dimensions undergoing a prescribed motion [5,6]. This research includes studying the effects of different types of motion and flow conditions on the propulsive performance and wake structures generated by the prescribed undulatory motion. This work also extends to fish schools, and studies by Pan et al. have shown the hydrodynamic interactions in a fish school using similar geometric simplifications [7,8].

It is well accepted that changing foil shape has been shown to greatly enhance performance in fixed and rotating foil

applications. In a previous study by Kelly et al., the effect of changing the foil shape in flapping foil propulsion has been shown to have significant effects on the hydrodynamics of the foil [9]. Most of the studies on fish-like undulation have utilized the NACA0012 standard foil shape to approximate a two-dimensional fish body or have selected a single fish body shape and used it for the study. However, no such study has been completed determining the effects of changing the fish body shape on the hydrodynamic performance of the fish swimming. This research aims to extend the study of the foil shape effect on the fish body in undulatory swimming simulations.

In this study, we prescribe an undulatory motion modeled after carangiform fish swimming to a variety of two-dimensional foil shapes. Computational fluid dynamics (CFD) simulations of these shapes are then completed using an in-house immersed boundary method-based DNS solver. The results of the simulations are used to study the effect of changing the fish body's maximum thickness, maximum thickness location, leading-edge radius, and boattail angle on the performance of the fish swimming. Additionally, the resulting flow fields are analyzed to determine the physical mechanisms behind the change in performance between the body shapes.

2. METHODS

2.1 Problem Definition

The fish body shape study begins by using the Class Shape Transformation (CST) parameterization method to create airfoil geometries. In this method, a class function defines the basic foil shape, and a shape function allows modification of that shape to create each foil. The method was developed by Kulfan et al. [10] and was chosen because previous studies identified it as an efficient method for foil shapes while maintaining core foil shapes [9, 11-12]. Based on the previous work of Han et al. [11], here, we similarly keep the class function the same and use six coefficients for the shape function (a_0, a_1, … a_5). The airfoil shape is derived as:

$$B_j = K_j^N \cdot x^{j+0.5} \cdot (1-x)^{N-j+1}, \quad (1)$$

$$K_j^N = \frac{N!}{j!(N-j)!}, \quad (2)$$

$$y(x) = \sum_{j=0}^{N} a_j \cdot B_j, \quad (3)$$

where B is the basis function, N is one less than the number of basis functions, and $y(x)$ defines the foil shape. The foil is then created by summing the product of each coefficient with the corresponding basis function. Additionally, in keeping with typical two-dimensional fish swimming studies, the standard NACA0012 foil shape will be utilized as a baseline shape for fish-like swimmers [7-8, 13].

Next, standard airfoil geometric parameters for symmetric airfoils are utilized to simplify the study and give meaning to the results of the study [9]. We have chosen to utilize the maximum thickness of the foil (δ_{max}), maximum thickness location along the foil (S_{max}), the leading-edge radius (α), and the boattail angle (β), shown in Fig. 1.

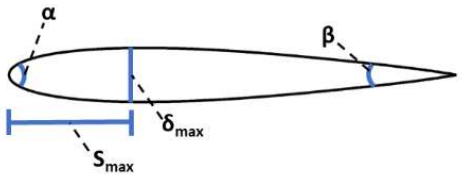

FIGURE 1: Airfoil Geometric Parameters.

The maximum thickness is defined as the width of the thickest part of the foil normalized by the length of the foil. The maximum thickness location along the foil is defined as the distance from the tip of the foil to the point of maximum thickness, normalized by the length of the foil. The leading-edge radius is defined as the radius of the arc formed by the front tip of the foil, normalized by the length of the foil. The boattail angle is defined as the angle created on the inside of the back tip of the foil.

Through the CST method, body shapes can be generated that maintain the core airfoil shape and allow for variation in each of the airfoil geometric parameters chosen. These foils can then undergo a prescribed motion to give the forward swimming undulatory motion.

Next, traveling wave kinematics are imposed on the foil to give carangiform undulatory motion. The motion follows the equation:

$$y(x,t) = A(x) \cdot \sin\left(\frac{2\pi}{\lambda}x - \frac{2\pi}{T}t\right), \quad (4)$$

where x and y are normalized by the body length of the foil, giving the head of the fish at x=0 and the tail at x=1. The value of $y(x,t)$ corresponds to the lateral deviation of the body of the fish from the original foil chord. T is the period of the traveling wave, and λ is the wavelength of the wave. $A(x)$ denotes the amplitude of the lateral motion and is expressed as a quadratic polynomial given by:

$$A(x) = a_2x^2 + a_1x + a_0, \quad (5)$$

where the coefficient values are chosen to be $a_2 = 0.02$, $a_1 = -.08$, and $a_0 = 0.16$, matching the previous study completed by Pan et al. [6].

2.2 Numerical Methods

The two-dimensional incompressible Navier-Stokes equations govern the flow in the numerical solver used and are written in index form and expressed in their nondimensional form as:

$$\frac{\partial u_i}{\partial x_i} = 0, \quad (5)$$

$$\frac{\partial u_i}{\partial t} + \frac{\partial u_i u_j}{\partial x_j} = -\frac{\partial p}{\partial x_i} + \frac{1}{Re}\frac{\partial^2 u_i}{\partial x_i \partial x_j}, \quad (6)$$

where the z terms are all zero, u_i are the velocity components, p is the pressure, and Re is the Reynolds number. The equations are discretized using a cell-centered, collocated arrangement of the primitive variables and is solved using a finite difference-based Cartesian grid immersed boundary method. The solver has been successfully implemented previously to canonical cases [14-15], biological flying and swimming [16-20] and validated for biological flows [21]. More information about the solver can be found in [22]. To understand our results, we first use the force coefficient in the x direction:

$$C_x = F_x/(0.5\rho U_\infty^2 c^2), \quad (7)$$

where F_x is the instantaneous net force in the x direction, ρ is fluid density, U_∞ is free stream velocity and c is the foil chord length. We then averaged C_x over one period of motion for each foil, giving $\overline{C_x}$, corresponding to the net force in the x direction over a cycle of motion. Similarly, the coefficients of thrust and power can be computed as:

$$C_T = F_T/(0.5\rho U_\infty^2 c^2), \quad (8)$$
$$C_P = P/(0.5\rho U_\infty^3 c^2), \quad (9)$$

where F_T is the instantaneous thrust and P is the instantaneous power consumed for the undulating motion. The averages over a period of motion are also computed, giving the results of $\overline{C_T}$, which is the net thrust over a cycle of motion, and $\overline{C_P}$, which is the net power consumed over a cycle of motion. Finally, the efficiency is calculated using a modified form of the Froude efficiency, which is defined as a ratio of useful power to total power:

$$\eta = \frac{\overline{C_T}}{\overline{C_T}+\overline{C_P}}. \quad (10)$$

The flow simulation is set up with the computational grid and boundary conditions shown in Fig. 2. For this study, the flow conditions are described by two dimensionless parameters, the Reynolds number (Re) and the Strouhal number (St), defined as:

$$\mathrm{Re} = \frac{U_\infty c}{\nu}, \quad (11)$$
$$\mathrm{St} = \frac{2fA}{U_\infty}, \quad (12)$$

where ν is the kinematic viscosity of the fluid, f is the tail beat frequency and A is the amplitude of the lateral motion at the tail tip. The Reynolds number is chosen to be 1,000 to mimic fish swimming. The Strouhal number is chosen to keep the cases near the free-swimming condition, where $\overline{C_x}$ is near zero, based on the NACA0012 foil baseline case. This results in a Strouhal number of 0.42, which gives the NACA0012 foil a $\overline{C_x}$ value of -0.0001.

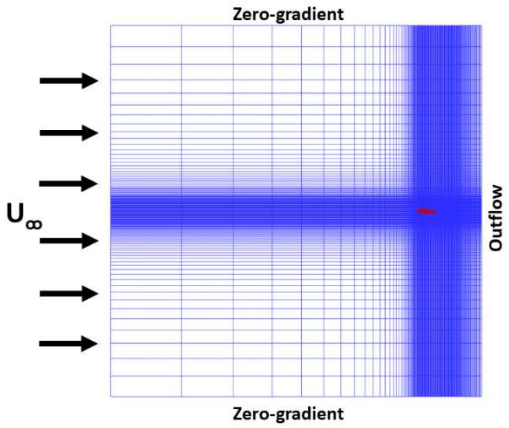

FIGURE 2: Cartesian grid and boundary conditions.

3. RESULTS

3.1 Hydrodynamic Performance

The hydrodynamic performance of each of the body shapes are computed using $\overline{C_T}, \overline{C_P}, \overline{C_x}$, and η as defined in the previous section. The results are shown in table 1. In the table, the body geometry and performance of the body shape resulting in a positive and negative change of each of the geometric parameters. In the final column, the difference in each body shape's efficiency compared to the baseline NACA0012 case is given, colored green if there is an improvement in performance and red if there is a decrease in performance.

In the table, changes in δ_{max} have the largest impact on the $\overline{C_x}$. For each of these cases, the overall body shape from the baseline foil is kept, but the shape is expanded in the lateral direction to give a larger and smaller thickness. From these results, we can determine that in free swimming conditions the thinner fish body shape moves faster than the thicker fish body, which follows intuition about hydrodynamic shapes. Additionally, a slight decrease in power consumed for the thinner fish body leads to an improvement in efficiency by about 4.0% from the thicker foil.

Next, increasing the maximum thickness location along the fish body is seen to have little impact on the performance of the fish. The thrust is slightly lower than the baseline case, and the power consumed also lowers giving no significant change in the efficiency. Decreasing the maximum thickness location along the body by moving the point of maximum thickness closer to the front of the body is shown to improve both the efficiency and the x force coefficient. The total change from the larger to the smaller maximum thickness location gives a 5.0% improvement in efficiency.

The changes in the leading-edge radius are shown in the table to lead to variation in both the x force coefficient and the efficiencies reached. Increasing the leading-edge radius, giving a rounder front edge of the foil, gives slightly improved thrust and power consumption, leading to a higher efficiency. Conversely, decreasing the leading-edge radius, giving a sharper front edge of the foil, gives a worse thrust, power consumption, and efficiency. The total change in efficiency from the thin to the

thick leading-edge radius on the fish body gives a 4.4% improvement in efficiency.

The changes to boattail angle show the largest impact on both the force coefficient in the x direction and the efficiency. Based on the $\overline{C_x}$ values, the thinner boattail angle would have a much higher velocity to reach a free-swimming state. The thinner boattail angle improves in all of the hydrodynamic parameters over the baseline case, and the thicker boattail angle performs worse in the thrust coefficient, force coefficient in the x direction, and the efficiency. The total change from the thick to the thin boattail angle gives a 10.2% improvement in efficiency.

TABLE 1: Cycle averaged thrust, power, force in x, and efficiency for each change in body shape. Body shapes shown are the limit of changes for each geometric parameter. Differences in efficiency are given relative to the NACA0012 baseline case.

Body Shape	*Body Geometry*	$\overline{C_T}$	$\overline{C_x}$	$\overline{C_P}$	η
NACA0012		0.222	~ 0	0.262	45.9%
Increased δ_{max}		0.218	-0.021	0.265	45.1% (-0.8%)
Decreased δ_{max}	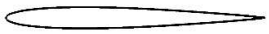	0.218	0.019	0.247	46.9% (+1.0%)
Increased S_{max}	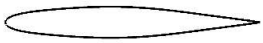	0.216	0.001	0.257	45.8% (-0.1%)
Decreased S_{max}	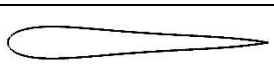	0.233	0.009	0.251	48.1% (+2.2%)
Increased α	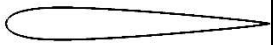	0.227	0.007	0.254	47.2% (+1.3%)
Decreased α		0.211	-0.006	0.256	45.2% (-0.7%)
Increased β	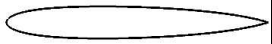	0.198	-0.026	0.258	43.3% (-2.6%)
Decreased β		0.234	0.022	0.253	48.0% (+2.1%)

3.2 Wake Structures and Surface Pressure in Varying Boattail Angle

From the cycle averaged coefficients shown in Table 1, it is apparent that changes in the boattail angle have the largest effect on the performance of the swimmer. To examine the physical mechanisms behind this result, we first look at the continuous coefficients of thrust and power through one cycle of motion, shown in Fig. 3. From the figure, we observe that the thrust generation is significantly improved for the thinner boattail angle at $0.3<t/T<0.6$. Additionally, a small improvement in power consumed is observed at $0.4<t/T<0.5$.

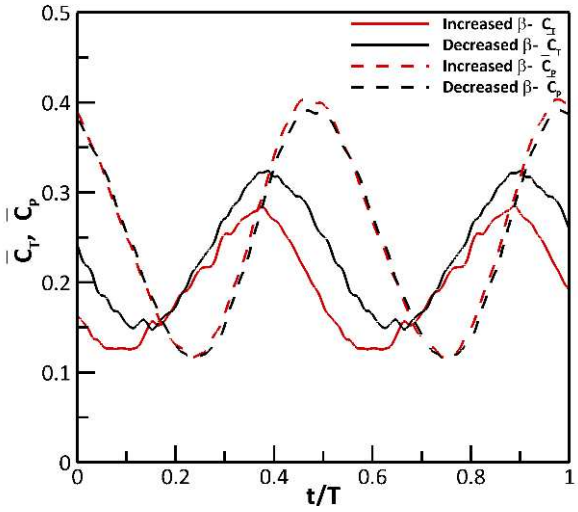

FIGURE 3: Continuous coefficients of thrust and power over one cycle of motion for increased and decreased boattail angle cases.

Next, to better understand the hydrodynamics behind this performance change the z-vorticity, ω_Z, is computed as the curl of the velocity. The results are plotted at $t/T = 0.42$, shown in Fig. 4. The time $t/T = 0.42$ is chosen to showcase the difference in both the power consumption and thrust seen in Fig. 3. In the figure, a secondary vortex is induced by the flow separation that occurs at the top of each of the foils. This separation is significantly larger in the case with the thinner boattail angle. In looking at the vorticity plots over a full cycle of motion, it is evident that the vortex is first generated when the tail is pointed downward, around $t/T = 0.13$.

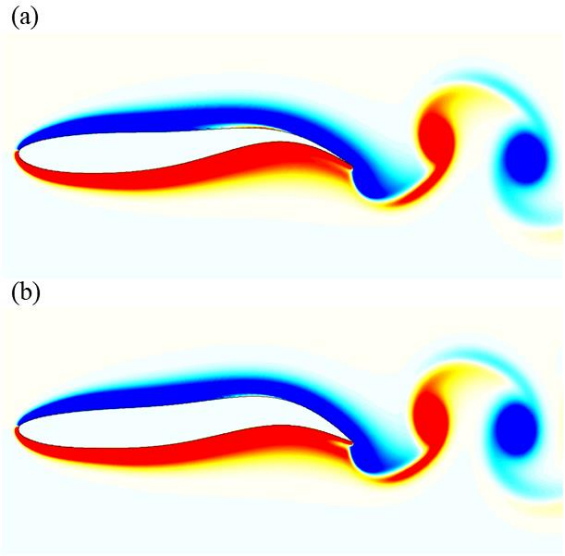

FIGURE 4: Vorticity (ω_Z) contour plots for the decreased (a) and increased (b) boattail angle cases

Because the boattail angle is smaller, the curvature is greater at this time step and the vortex is generated sooner in the motion and grows to a larger size as seen in Fig. 4. At the time shown in

the figure, the back region of the foil is just starting to rise above the middle of the foil on the top edge. Because of the secondary vortex, this motion consumes less power in the thinner boattail angle case. The reduction in power consumption can be seen from this time until $t/T = 0.50$ in Fig. 3. As the body completes its upward motion, the secondary vortex is no longer advantageous and the power consumption returns to about the same values.

In order to better understand the enhancement in thrust generated by the thinner boattail angle, the coefficient of pressure is computed:

$$C_{pr} = p/(0.5\rho U_\infty^2). \quad (13)$$

The results are shown in Fig. 5, which shows the distribution of the pressure coefficient on the surface of the body.

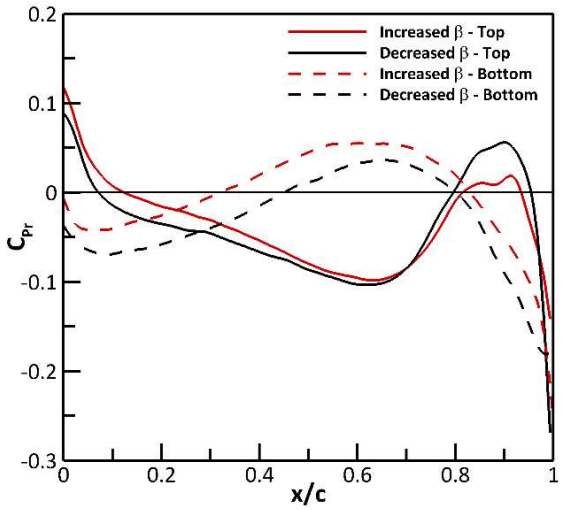

FIGURE 5: Pressure coefficient (C_{pr}) distribution along the top and bottom surfaces of the increased and decreased boattail angle cases

In Fig. 5 it is very evident that the top of the body has a large increase in the surface pressure at $0.8<x/c<0.95$. In Fig. 4 the normal to the surface in this region has a significant component in the *x-direction*. Because of this, the higher pressure on that surface increases the force in the *-x* direction, leading to the enhanced thrust observed in Fig. 3 at the current time. This combination of increased pressure and a surface normal component in the *-x* direction is observed at times $0.3<t/T<0.6$, which corresponds to the time range for increased thrust generation observed in Fig. 3.

To better understand the cause for this increased pressure region, the contours of the pressure coefficient near the fish body are plotted in Fig. 6. As expected, a region of higher pressure is observed on the top trailing edge of the thinner boattail angle body that is not seen in the thicker boattail angle case. In looking at the pressure contour plot throughout a cycle of motion, it is observed that the high-pressure region shown is generated early in the cycle, around $t/T = 0$. At this time, the curvature along the top edge of the foil is greater in the thinner boattail angle case, which causes the high-pressure region to develop sooner. As the high-pressure region moves along the body, the thinner boattail angle case maintains a higher pressure that becomes advantageous as the tail turns downwards and the surface normal has a component in the *-x* direction.

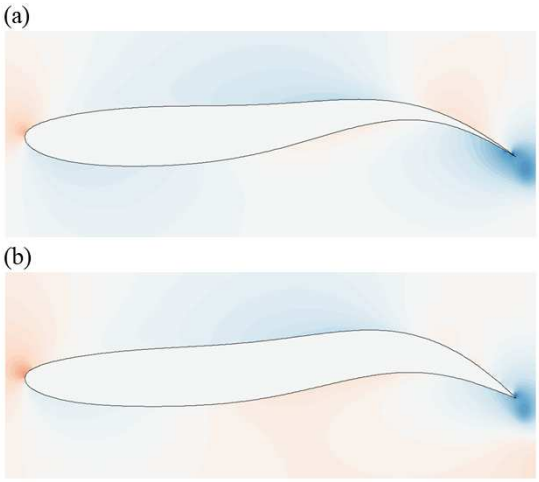

FIGURE 6: Pressure coefficient (C_{pr}) contour plots for the decreased (a) and increased (b) boattail angle cases

4. CONCLUSION

In this research, two-dimensional numerical simulations were completed using an immersed boundary method to investigate the effect of body shape on the performance of undulatory swimmers. Particular focus was given to each geometric shape parameter used to describe symmetric foils: maximum thickness, maximum thickness location, leading-edge radius, and boattail angle. It was found that changes in maximum thickness, maximum thickness location, and leading-edge radius all lead to a total change in the efficiency of 4-5%. Changes in the boattail angle led to efficiency changes of over 10%. Analysis of the pressure and vorticity showed that the primary reason for the improved performance with a thinner boattail angle is due to the increased curvature around the middle of the fish body that leads to a high-pressure region at the tail giving an improvement in thrust generation. Additionally, power consumption savings are gained due to the formation of a larger secondary vortex, also occurring because of the higher curvature in the middle of the body.

ACKNOWLEDGEMENTS

This work was supported by ONR MURI N0014-14-1-0533, NSF CNS -1931929, the NSF NRT program, and ASME FED GSS.

REFERENCES

[1] White, C., Lauder, G., and Bart-Smith, H. "Tunabot Flex: A Tuna-Inspired Robot with Body Flexibility Improves High-Performance Swimming." *Bioinspiration and Biomimetics* 16, no. 2 (2021).

[2] Wang, J., Wainwright, D., Lindengren, R., Lauder, G., and Dong, H. "Tuna Locomotion: A Computational Hydrodynamic Analysis of Finlet Function." *Journal of the Royal Society Interface* 17, no. 165 (2020).

[3] Liu, G., Ren, Y., Dong, H., Akanyeti, O., Liao, J., and Lauder, G. "Computational Analysis of Vortex Dynamics and Performance Enhancement Due to Body-Fin and Fin-Fin Interactions in Fish-like Locomotion." *Journal of Fluid Mechanics* no. 829 (2017): 65–88.

[4] Han, P., Liu, G., Ren, Y., and Dong, H. "Computational Analysis of 3D Fin-Fin Interaction in Fish's Steady Swimming." *FEDSM2016*, 2016: 1–6.

[5] Khalid, M., Wang, J., Dong, H., and Liu, M. "Flow Transitions and Mapping for Undulating Swimmers." *Physical Review Fluids* 5, no. 6 (2020): 63104.

[6] Verma, S., Novati, G., and Koumoutsakos, P. "Efficient Collective Swimming by Harnessing Vortices through Deep Reinforcement Learning." *Proceedings of the National Academy of Sciences of the United States of America* 115, no. 23 (2018): 5849–54.

[7] Pan, Y., Han, P., Huang, J., and Dong, H. "Effect of Formation Pattern on Schooling Energetics in Fish-Like Swimming." *FEDSM2020,* 2020, 1–8.

[8] Pan, Y., and Dong, H. "Computational Analysis of Hydrodynamic Interactions in a High-Density Fish School." *Physics of Fluids* 32, no. 12 (2020).

[9] Kelly, J., Han, P., Dong, H., and Van Buren, T. "Wake Structures and Effect of Hydrofoil Shapes in Efficient Flapping Propulsion." *FEDSM2021*, 2021: 1–7.

[10] Kulfan, B., and Bussoletti, J. "'Fundamental' Parametric Geometry Representations for Aircraft Component Shapes." *Collection of Technical Papers - 11th AIAA/ISSMO Multidisciplinary Analysis and Optimization Conference* 1 (2006): 547–91.

[11] Han, P., Bode-Oke, A., Dong, H., Van Buren, T., Floryan, D., and Smits, A. "Comparison of Geometric Parameterization Methods for Optimal Shape Design in Efficient Flapping Propulsion." *AIAA AVIATION Forum* (2019): 1–8.

[12] Masters, D., Taylor, N., Rendall, T., Allen, C., and Poole, D. "Geometric Comparison of Aerofoil Shape Parameterization Methods." *AIAA Journal* 55, no. 5 (2017): 1575–89.

[13] Dong, G., and Lu, X. "Characteristics of Flow over Traveling Wavy Foils in a Side-by-Side Arrangement." *Physics of Fluids* 19, no. 5 (2007).

[14] Han, P., Pan, Y., Liu, G., and Dong, H. "Propulsive Performance and Vortex Wakes of Multiple Tandem Foils Pitching In-Line." *Journal of Fluids and Structures* 108 (2022): 103422.

[15] Dong, H., Liang, Z., and Harff, M. "Optimal Settings of Aerodynamic Performance Parameters in Hovering Flight." *International Journal of Micro Air Vehicles* 1, no. 3 (2009): 173–81.

[16] Dong, H., and Liang, Z. "Effects of Ipsilateral Wing-Wing Interactions on Aerodynamic Performance of Flapping Wings." *48th AIAA Aerospace Sciences Meeting Including the New Horizons Forum and Aerospace Exposition*, no. January (2010): 1–7.

[17] Koehler, C., Wischgoll, T., Dong, H., and Gaston, Z. "Vortex Visualization in Ultra Low Reynolds Number Insect Flight." *IEEE Transactions on Visualization and Computer Graphics* 17, no. 12 (2011): 2071–79.

[18] Bode-Oke, A., Zeyghami, S., and Dong, H. "Aerodynamics and Flow Features of a Damselfly in Takeoff Flight." *Bioinspiration and Biomimetics* 12, no. 5 (2017).

[19] Menzer, A., Gong, Y., Fish, F., and Dong, H. "Bio-Inspired Propulsion : Towards Understanding the Role of Pectoral Fin Kinematics in Manta-like Swimming," *Biomimetics* 2022, 7, 45.

[20] Ren, Y., Dong, H., Deng, X., and Tobalske, B., "Turning on a Dime: Asymmetric Vortex Formation in Hummingbird Maneuvering Flight." *Physical Review Fluids* 1, no. 5 (2016): 2–4.

[21] Wang, J., Ren, Y., Li, C., and Dong, H. "Computational Investigation of Wing-Body Interaction and Its Lift Enhancement Effect in Hummingbird Forward Flight." *Bioinspiration and Biomimetics* 14, no. 4 (2019).

[22] Bozkurttas, M., Dong, H., Seshadri, V., Mittal, R., and Najjar, F. "Towards Numerical Simulation of Flapping Foils on Fixed Cartesian Grids." *43rd AIAA Aerospace Sciences Meeting and Exhibit - Meeting Papers*, no. December 2014 (2005): 15801–9.